Surface indentation arrays for high-throughput analysis of viscoelastic material properties

Peter M. Johnson and Christopher M. Stafford
Polymers Division, National Institute of Standards and Technology, 100 Bureau Drive, Gaithersburg, Maryland 20899, USA

(Received 3 September 2009; accepted 23 September 2009; published online 30 October 2009)

Viscoelastic relaxation processes factor into polymer performance and stability throughout an application lifetime, controlled by the polymer network structure and dynamics which occur over a wide spectrum of time scales. In this work, we detail the design and operation of an independent array of surface indenters which can measure the creep response at multiple points on a polymer substrate. Samples with composition and temperature gradients are used to exhibit the ability to measure viscoelastic properties under unique conditions for each indentation. Methacrylate photopolymer systems are measured at different compositions and crosslink densities simultaneously within an indenter array to increase the measurement throughput, with a measured creep compliance ranging from 10^{-9} Pa^{-1} to 10^{-5} Pa^{-1}. The application of temperature gradients allows for the viscoelastic measurements to be assembled onto a master curve using time-temperature superposition. © *2009 American Institute of Physics.* [doi:10.1063/1.3247905]

I. INTRODUCTION

Relaxation processes in viscous liquids and glasses have been studied extensively as these processes dictate polymer reliability in applications where a constant or cyclical load is applied. These relaxation processes lead to permanent deformation and potentially ultimate failure of the sample, but the causes of glassy behavior and relaxation kinetics in polymeric systems remain a major unsolved area of condensed matter physics.[1,2] Since viscoelastic processes require significant time to measure, the ability to rapidly screen these relaxations is limited since these processes occur at both short and long time scales. Viscoelastic properties are commonly measured by rheometers, tensile stress/strain measurements, and indentation techniques, which range from nanoindenation to larger macroscale systems. For these experimental designs, two methods exist to increase experimental throughput: sensor multiplexing and time-temperature superposition. For sensor multiplexing, the same experimental design is replicated to build multiple sample stations which can each measure one sample of the same material, but the infrastructure and time cost preclude this experimental design due to the complexity of the measurement method. The other alternative, time-temperature superposition, is a measurement independent technique which measures samples at different temperatures and then shifts these results with respect to a reference temperature. This method can predict viscoelastic properties on time scales that are otherwise difficult to measure experimentally using relatively short experimental times.

Sensor multiplexing methods rely on automated techniques where experiments are performed sequentially. In the case of rheometry or mechanical testing, equipment must be replicated and the measurement of large sample arrays is difficult due to the equipment cost and experimental time required. For indentation techniques, automated processes such as nanoindentation have the potential to screen the viscoelastic response at multiple individual points, but in a serial fashion. Limitations arise for viscoelastic experiments, since the time required to measure material response in a serial fashion and equipment stability prevents performing measurements at long time scales. Moreover, specialized adaptations are required if environmental conditions are varied due to the sensitivity of the measurement.[3–6] For techniques with simultaneous or parallel measurements, the number of force and distance sensors required constrains sample sizes to be equivalent as defined by the measurement geometry. The limited time scale and design requirements to measure systems at different environmental conditions can also present limitations to the range of experimental tests that can be performed.[7]

Conversely, time-temperature superposition principles can be applied to measure viscoelastic material responses that occur at times exceeding the limitations of experimental equipment. To create an accurate master curve using time-temperature superposition, shift factors must be known from prior experimentation or predictive theories such as the Williams–Landel–Ferry (WLF) theory. WLF theory predicts shift factors based on a linear increase in free volume with respect to temperature, and these factors have been calculated for a wide range of bulk commodity polymers.[8] WLF shift factors are generally valid for samples above the glass transition temperature, but free volume changes near the glass transition temperature can cause shift factors to deviate. With more complex systems such as polymer blends and composite materials, viscoelastic responses occur in multiple distinct time domains due to interfacial regions, blend composition, and filler interactions.[9–12] This complexity can prevent simple models from accurately predicting WLF shift factors for time-temperature superposition, as is the case for systems with nonlinear free volume changes.[13]

While predictive models exist for time-temperature superposition of more complex systems, these models contain a large number of unknown constants or empirical fits based on prior experimental results.[14] Without reliable predictions, experiments utilizing time-temperature superposition are required to analyze the full viscoelastic response of the system, calculating the shift factors to obtain the resulting time-shifted creep compliance curve. For certain systems, shift factors are complicated by the additional need for vertical shifts of the compliance on top of the standard shift factors with respect to time, requiring longer and more extensive experiments to assemble measurements onto a master curve.[15] Since these measurements require a high number of experimental measurements, a parallel analysis technique with the ability to control individual sample temperatures would allow master curves and their resulting shift factors to be determined within a single experimental scan. To address this measurement need, we demonstrate a simple, high-throughput method to measure creep compliance of polymer films using an array of independent spherical indenters. This system is then adapted to analyze combinatorial libraries with composition or temperature gradients, allowing for parallel measurements that enable analysis of the viscoelastic response of complex materials systems.

II. EXPERIMENTAL SETUP AND OPERATION

A. Sample geometry

Equipment, instruments or materials are identified in the paper in order to specify the experimental details adequately; any mention of commercial products is for information only. Such identification does not imply recommendation by National Institute of Standards and Technology (NIST), nor does it imply the materials are necessarily the best available for the purpose. Uncertainties in this paper are given by standard error with 95% confidence intervals unless noted. For viscoelastic indentation measurements, either the applied load or indenter depth is fixed while the other parameter is monitored as a function of time. This measurement is then related to the viscoelastic response of the polymer substrate as relaxation processes in the polymer network reduce the applied load or increase the indenter depth. The contact geometry for this technique uses a sphere on a planar surface, with the load force from gravity acting to indent the polymer substrate [Fig. 1(a)]. Since the modulus of the sphere is much greater than the modulus of the polymer substrate, the indentation can be simplified further to a Hertzian contact where the indentation of the sphere forms a circular contact area between the surface and the sphere. This indentation geometry has been well studied in a variety of orientations and systems, ranging from macroscale experiments on concrete to indentation of nanometer size features.[4,5,16] With the geometry described here, each sphere acts as a constant, fixed force load on the surface, and the contact area provides a measure of the extent of indentation.

For this method, the contact area between the sphere and the substrate was observed via optical microscopy, simplifying sensor multiplexing since indenter contact area was determined from the image and the applied force was a known

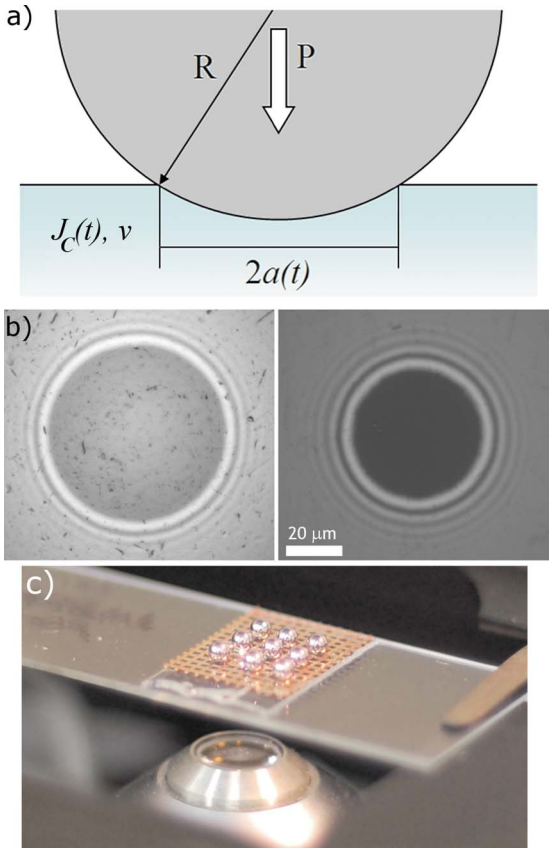

FIG. 1. (Color online) (a) Schematic of indenting geometry for a single sphere on a polymer surface, where the radius, R, and load, P, are known from the sphere properties. The contact radius, a, determines the shear compliance, J_C, of the polymer substrate. (b) Microscope images of a contact areas from two different sphere types on the same sample substrate with contact diameter of 62 μm and 44 μm. (c) View of an indenter array on a polymer surface, without the attached motion stage.

fixed value. The optical fringes seen in Fig. 1(b) are an interference pattern commonly called Newton's rings, which is caused by the reflection of light between a spherical surface and an adjacent flat surface. The optimal contact radii ranged from 8 to 150 μm, which was limited by the resolution of the contact area detection method and the limits of the Hertzian contact model. This problem had been solved in prior work by Lee and Radok for a rigid elastic indenter and a viscoelastic substrate.[17] The creep compliance, $J(t)$, for a step load stress response is calculated by

$$J(t) = \frac{8a(t)^3}{3RP(1-v)}, \tag{1}$$

where a is the contact radius, R is the indenting sphere radius, P is the load from gravity caused by the mass of the indenter, and v is Poisson's ratio. The indenter load is calculated from the mass of the indenting sphere, which is dependent on the radius and density of the sphere. Measurements of creep compliance using spheres of different radii or density confirmed the applicability of the model by producing statistically equivalent creep compliance values. To build an additional sensor for this geometry, the only requirements were to add an additional sphere on the surface and to enter a corresponding position in the microscope capture sequence.

Since metallic spheres have many industrial applications, a wide range of material, sphere radius, and hemispherical shapes were available. The variety in available spheres provided options to change the static load and radius, which shifts the range of measurable compliance values while still maintaining Hertzian contact mechanics. These two parameters allow the experimental design to match the correct sphere type to the expected compliance range. To ensure the measurement of bulk properties in these experiments, a thickness of greater than 0.75 mm was used in all cases to prevent polymer-support interactions at the interface and to allow the application of Hertzian contact mechanics with no correction factors. Experiments on different substrate thicknesses greater than 0.75 mm showed no statistical changes in the measured creep compliance, and for higher compliance measurements a contact radius to sample thickness ratio of less than 0.1 was maintained for all experiments.

B. Sample and indenter preparation

Transparent polymer substrates were required for this experimental design to image the contact area for each sphere. Substrates needed to be level and smooth to ensure circular contact areas and to prevent contact area drift. Spheres were cleaned in water and acetone and then air dried prior to indentation. The spheres were then brushed with an optical cleaning cloth to remove any stray particles prior to being placed into the array. Tests on different sphere sizes and material were performed using chrome steel, glass, and sapphire spheres of different radii, with statistically equivalent creep compliances provided the radius to thickness ratio was within the limits stated above. These changes to the sphere material and radius shift the measured compliance at the same contact radius by up to two orders of magnitude. Chrome steel spheres were used for all experiments shown here due their inexpensive cost for high sphere quality. All spheres released from the surface with minimal effort, with spheres falling off the sample when tilted from a horizontal position. In the case of strongly adhesive and compliant polymer systems, the contact area will be distorted and adhesion effects must be accounted for. No system studied within this work exhibits these effects.

An array of nine indenters was assembled on a holding platform to measure multiple positions on the polymer substrate, with sphere spacing dependent on the sphere size and regions of interest. This platform was attached to a manual motion stage, which allowed for the spheres to be lifted to and from the surface. Holes in the platform were slightly smaller than the diameter of the sphere; this facilitated the placement and removal of the spheres from the surface. The holding platform was made from 1 mm thick metal stock and detachable from the motion stage so other platforms with different sphere sizes or array spacing could be utilized. Since the diameter of the platform holes was slightly smaller than the sphere diameter, the spheres do not contact the holding platform after being lowered to the polymer surface. The penetration depth of the sphere into the polymer is less than 10 μm, so contact with the edge of the platform would occur only if the sphere significantly moves once placed on the surface. The center point of the contact region is monitored to detect if this ever were to occur.

Experiments were performed with an array of nine 1.19 mm radius chrome steel spheres with a sphere spacing of either 3.5 or 7 mm [Fig. 1(c)], depending on the polymer substrate sample size. In all experiments, the contact time begins when the sphere array is lowered to the surface, which creates the initial indentation at each sphere location. The applied force of each sphere from mass measurements was $0.54211\ \mathrm{mN} \pm 0.00004\ \mathrm{mN}$ assuming standard gravitational forces. With these parameters for indenter radius and load, the compliance measurement range using the stated contact radius range was from $7.5 \times 10^{-10}\ \mathrm{Pa}^{-1}$ to $4.9 \times 10^{-6}\ \mathrm{Pa}^{-1}$. Compliances measured by individual spheres exhibited no statistical deviations as compared to the individual averages when tracked over multiple repeated experiments.

C. Image collection and processing

Image sequences were collected using an inverted microscope (Leica DMIRE2) at 20× magnification with a computer controlled x-y stage (Leica DMSTC). A LABVIEW (National Instruments) interface was implemented to control stage positioning and image sequence timing, with image collection through IMAGE PRO software (Media Cybernetics). Prior to image collection, the image capture positions were checked to ensure that the contact area was within camera view, requiring 30 s of contact time on average before image collection begins. Once image collection began, each image was stored with an associated contact time starting from when the array was placed on the surface. Image sequencing of a square array was measured in a spiral sequence to minimize rastering time between sphere contact images. The array was imaged sequentially over the time period, with equivalent logarithmic time steps dictating when array image sequences should be taken to prevent unneeded image processing at long times. At shorter times, time steps were smaller than the time required to image the array, and image sequences were immediately started with no time delay when this occurred. Experiments were performed for up to 68 h with 80–100 array image sequences, and all experiments were performed at 22 °C unless otherwise noted.

A standard high-throughput experimental scan resulted in 720 images, 80 images per sphere, and a text file containing the contact time for each image in the sequence. A program was developed in MATLAB to automate the detection of the contact area in each image and determine contact radii for each individual sphere using a circular Hough transform, which is a technique used to detect circular or other definable shapes. A circular Hough transform assumes that edge detected points are positions on the edge of a circle and transforms them into a new position space defined by the parameters of a circle.[18,19] The edge detected points were transformed from the (x,y) position on the edge of a circle to parameters required for drawing a circle: the center point (x_0,y_0) and contact radius (a) using an equation for a circle [Eq. (2)],

$$(x - x_0)^2 + (y - y_0)^2 = a^2. \quad (2)$$

For each image, Canny edge detection was performed to detect all edge pixels in the sample, which included the edge of the contact area.[20] The edge of the contact area is at the inner edge of the first interference ring. To calculate the transform, all possible center positions for each detected edge point were calculated for a given radius, and these positions were incremented in a matrix which represented possible center point positions. Once this is repeated for every edge pixel, each position in the center point matrix contains the number of edge points where a circle of the specified radius would occur. The center point matrix was normalized by the circumference pixels of a circle with that radius, so each value could be considered the detected fraction of a circle at that center point and radius. In the case of an image with a single perfect circle, only one position would have a value equal to one in the center point matrix but only if the correct radius was chosen.

Center point matrices for a range of radii were calculated for each image, with the highest detected fraction chosen as the correct center point and radius. This process can be computationally intensive, but the processing of these image sequences was reduced by image cropping and radius prediction techniques. Since the contact area of one sphere appeared in the same position for all images, the Hough transform region was reduced to an area immediately around the center point once the first contact area had been detected. In addition, the contact radius of the previous image provided a lower bound for the contact radius of the current image and the rate of change was monitored to expand the upper radius limit as necessary. Contact images over the optimal range of contact radii were taken with monochromatic light and then analyzed to determine contact radii using the described analysis protocol. With the measured contact radius and wavelength of the monochromatic light, predicted interference fringe patterns of a sphere and a flat plane were produced and compared to the contact images. The predicted interference fringes matched the contact images, confirming the image analysis technique was correctly indentifying the contact radius.

Image sequences from an experiment were processed in under 15 min, and a minimum detected circle fraction was set at 0.4 to indentify noncircular contact areas or poor quality images. A list of center position, contact radius, and elapsed time for each sphere in the array was reported and then used to calculate compliance for each sphere. The uncertainty of the contact radius measurement contributed a majority of the error for this technique, ranging from 1% to 5% of the measured compliance value, decreasing in magnitude as the contact radius increases. The center point was tracked to check for sphere drift, and a random drift of less than 3 μm was observed for 68 h sequences. No spheres exhibited center point drift in a single direction that would indicate contact with the edge of the holding platform. If contact times before 30 s were needed, the array could be lowered to the surface and one contact area imaged repeatedly for 60 s. These images were then processed using the same contact area detection program and integrated into the larger time sequence.

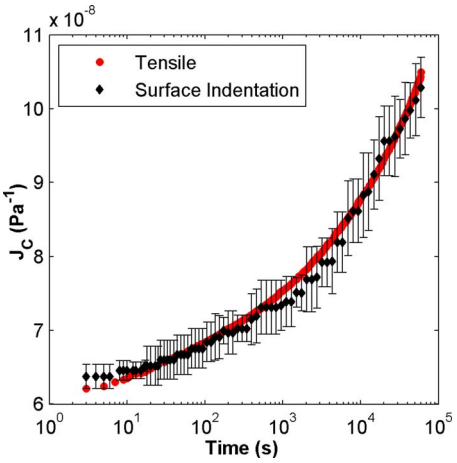

FIG. 2. (Color online) Kraton creep compliance measured over 16.7 h using surface indentation and tensile creep measurements. Both experiments were performed at 22 °C, with error bars removed from the tensile experiment for clarity. Error bars are standard error with 95% confidence intervals.

D. Comparison to tensile creep measurements

To confirm the accuracy of the technique and measurement design, experiments were performed on a commonly available polymer to facilitate comparison to other viscoelastic measurement techniques. Poly(styrene-ethylene/butylene-styrene) triblock copolymer (SEBS) with a mass fraction of 30% styrene (Kraton Polymers LLC, Kraton G1650M) was investigated with both the surface indentation technique and tensile creep experiments. SEBS samples were solvent cast in toluene and left under vacuum for 24 h to remove any remaining solvent. The polymer film thickness was approximately 1 mm, and thicker films were created by repeating the solvent casting process. Each prepared sample was sectioned into specimens of appropriate size for both surface indentation and tensile creep experiments.

Tensile experiments were performed with a Texture Analyzer (model TA.XT2i, Texture Technologies Corp.) in tension mode at a constant strain, measuring force as a function of time. Sample dimensions were $10 \times 1 \times 25$ mm^3, with a 3% strain held for 16.7 h at a temperature of 22 °C. New samples were used for each tensile experiment, and the storage modulus, $E(t)$, was converted to an equivalent compliance, $J(t)$, using a Poisson's ratio of 0.49. Compliance curves for the SEBS system are shown in Fig. 2 using surface indentation and standard tensile creep experiments.

Both tensile and surface indentation techniques resulted in statistically equivalent creep compliance over the entire time period analyzed. Creep compliance at 5 s was measured as 6.37×10^{-8} Pa^{-1} $\pm 2.0 \times 10^{-9}$ Pa^{-1} for surface indentation as compared to 6.21×10^{-8} Pa^{-1} $\pm 1.3 \times 10^{-9}$ Pa^{-1} from tensile creep measurements. Higher standard error for surface indentation was attributed to the error in the radius detection process. Both experimental techniques reached equivalent compliance at 16.7 h, with 1.03×10^{-7} Pa^{-1} $\pm 5.1 \times 10^{-9}$ Pa^{-1} for surface indentation and 1.05×10^{-7} Pa^{-1} $\pm 2.3 \times 10^{-9}$ Pa^{-1} for tensile creep.

Tensile creep compliance measurements for this specific SEBS polymer has also been measured by Rek *et al.*,[21] with values for tensile creep compliance comparable to the results shown here.

III. GRADIENT MEASUREMENT TECHNIQUES

A. Composition gradients

Since SEBS samples exhibited a limited range of compliance, a second set of experiments tested photopolymer substrates that could be designed to provide a broad range of creep compliance measurements. These experiments were also designed to demonstrate the application of various gradients to change the local properties of the polymer substrate under each indenting sphere. Photopolymers are used in a variety of processing and end use applications, including adhesives, lithography, coatings and biomaterials. These applications require a wide range of mechanical properties to meet specific needs and environments, ranging from high strength adhesives to soft hydrogel networks. The broad range of chemical moieties available for photopolymerization enables the design of materials with a variety of viscoelastic responses. In the case of pressure sensitive adhesives, long linear chains are lightly crosslinked to improve creep resistance while maintaining other critical mechanical properties. At the other end of the spectrum, adhesive photopolymers require highly crosslinked, high modulus materials for high load applications.

The systems studied here were binary or ternary systems containing isobornyl methacrylate (IBoMA), lauryl methacrylate (LMA), and 1,6-hexanediol dimethacrylate (HDDMA). Binary systems of IBoMA and LMA result in a sample comprised of linear polymer chains whose viscoelastic properties are dependent on the fraction of the two monomers. The addition of HDDMA to the formulation as a crosslinker would increase the molecular mass of the network and inhibit chain mobility. To polymerize these samples, the photoinitiator 2,2-dimethoxyacetophenone was used at a mass fraction of 0.5% in all samples, while the composition of the monomers was varied in order to modulate the creep compliance of the system. The monomer formulation was cured between glass slides producing $\approx$1 mm thick samples using an Acticure 2000 mercury arc lamp (EXFO Systems) with a 365 nm bandpass filter at a light intensity of 10 mW/cm^2 for 3600 s.

In order to further demonstrate the high-throughput capability of our experimental design, step gradients in composition were fabricated in order to measure different polymer formulations at each indentation point on the sample. To produce a step composition gradient, the first composition was polymerized between two glass slides with 1 mm Teflon spacers. After curing the first composition using the previously described conditions, one spacer was moved 4 mm to create an opening next to the cured polymer, and another monomer formulation in the sequence was polymerized next to the cured sample. Cured regions were covered from the light to prevent differences in exposure time. Polymer formulations were randomly ordered to ensure cured regions were consistent regardless of order. After curing, samples were left for 48 h in the dark before experiments were performed to finish any remnant polymerization caused by extant radicals. The creep compliance for the LMA/IBoMA composition gradient is shown in Fig. 3.

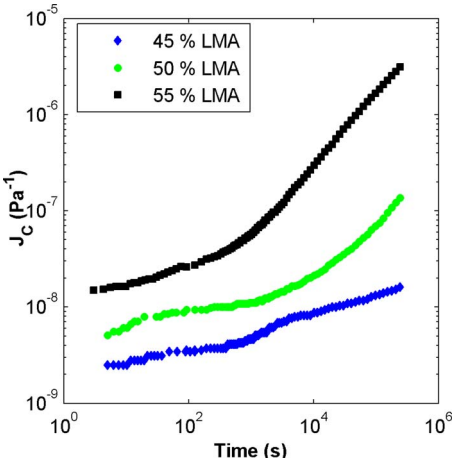

FIG. 3. (Color online) Creep compliance measured to 68 h using surface indentation on a step gradient comprised of three formulations: 45/55%, 50/50%, 55/45% LMA/IBoMA by mass fraction. Measurements were performed simultaneously on all three compositions at 22 °C, with error bars smaller than the data points. Error bars are standard error with 95% confidence intervals.

Creep compliance of these polymer systems ranged over three orders of magnitude, from 2.2×10^{-9} Pa^{-1} to 2.4×10^{-6} Pa^{-1}. As the amount of LMA increased in the polymer, the compliance increased due to a reduction in the glass transition temperature, with each section having a significantly different compliance for all measured times. This compliance range encompasses most common polymer systems at their end use application range, excluding viscous polymer melts at high compliance values and glassy polymer systems at low compliance values. For highly crosslinked networks, differences in creep compliance were too small and slow to measure with this technique at room temperature. These formulations were developed to have glass transition temperatures near the experimental temperature and produce systems with a wide range of compliance. The change in the rate of creep compliance over time was indicative of glass transition effects caused by broad polymer chain length distribution inherent in photopolymerized networks.

To investigate the effect of network architecture, small amounts of the dimethacrylate crosslinker, HDDMA, were added to the 55/45% mass fraction LMA/IBoMA formulation prior to polymerization. The addition of HDDMA increased the molecular mass of the network by linking linear polymer chains together, decreasing chain mobility and retarding viscoelastic relaxations. The compliance measurements of the polymer with different crosslinker concentration are shown in Fig. 4.

With the addition of 0.5% HDDMA, there was a significant reduction in creep compliance at longer times while the rate of creep was statistically equivalent. The polymer sample with no HDDMA was statistically equivalent to the previous step gradient sample with a mass fraction of 45% LMA, replicating the prior experiment throughout the entire experimental time. While the initial creep compliance was

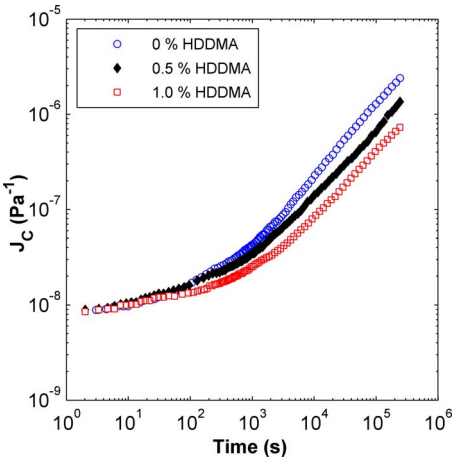

FIG. 4. (Color online) Creep compliance measured to 68 h using surface indentation on a step gradient consisting of three formulations: 55/45% mass fraction LMA/IBoMA with 0%, 0.5%, and 1% mass fraction HDDMA. Measurements were performed simultaneously on all three compositions at 22 °C, with error bars smaller than the data points. Error bars are standard error with 95% confidence intervals.

similar in all formulations, samples containing HDDMA exhibited lower compliance at shorter times. The difference in compliance at longer times was predominately due to the slower change in creep compliance at shorter times, leading to a lower overall compliance by the end of the experiment. This reduction in creep compliance was distinguishable as early as 100 s, with an ultimate reduction in compliance at 68 h from 2.4×10^{-6} Pa^{-1} to 7.3×10^{-7} Pa^{-1}. The long experimental time explored here allowed for an in-depth analysis of multiple polymer networks simultaneously. This approach can also be easily scaled up to include additional indenters to increase throughput. Each additional sphere increases the time for a single image array sequence, so the initial time resolution between image sequences is decreased. However at long times, the small increase in imaging time due to additional spheres is small compared to the interval between time points. For the experiments described here, increasing the array to twelve spheres would impact the capture times for images taken before 1200 s. To test the viscoelastic response of a glassy system which exhibits slow viscoelastic properties at room temperature, polymer samples could be tested at elevated temperatures then shifted using time-temperature superposition as described in the next section.

B. Time-temperature superposition

Time-temperature superposition can be used to extend the range of creep compliance measured by time shifting compliance measurements taken at different temperatures to a common reference temperature, enabling faster measurements of time points outside of the standard experimental design. Thus, a gradient in temperature further enhances the high-throughput capability of our experimental design. A temperature gradient was developed on a 50/50% IBoMA/LMA by mass photopolymer substrate, measuring compliance over shorter times at various temperatures to develop a master curve. The assembly for generating temperature gradients is given in detail elsewhere, but briefly, a hot block and a cold block were attached to a quartz slide with a 600 μm photopolymer sample already polymerized on the slide.[22] The bottom of the slide was insulated except for the region around the photopolymer substrate to allow imaging of the indenter array. The hot element consisted of a flexible heater with an insulating cover attached 3 mm from the edge of the polymer substrate. The flexible heater was controlled with a Variac, and the hot block temperature was varied from 50 to 85 °C, depending on the required temperature gradient. The cold block, an aluminum block cooled by drawing ambient air through the center of the block, was attached 3 mm from the edge of the opposite edge of the polymer sample. Temperature was monitored through embedded thermocouple probes at three positions on the polymer sample; these positions corresponded to the row locations in a 3×3 sphere array. Experiments were performed at temperatures ranging from 22 to 55 °C, with a maximum gradient temperature range of 1.2 °C/mm.

Larger array spacing was employed here to obtain a greater temperature difference between rows. During the equilibration period, the sphere array was placed on the sample to ensure the spheres were equilibrated to the same temperature as the substrate. When the temperature gradient had stabilized according to the temperature probes, the sphere array was lifted and moved slightly in the direction orthogonal to the temperature gradient. Temperatures in the polymer substrate were monitored throughout the experiment, with a variation of less than 0.3 °C during the experiment. When placed back on the sample, each sphere contacted a new region of the polymer substrate, and the compliance experiment was performed in the same manner as described previously. Since the sphere exerts a static force, the effect of the sphere temperature on the viscoelastic measurement was limited to any heat transfer at the interface of the contact zone. By equilibrating the sphere temperature beforehand and minimizing the contact area at the interface, any local change in temperature was minimized. This temperature change was significant if room temperature spheres were placed on the surface (no equilibration step), resulting in measured compliance values that were impossible to fit with a single shift factor. The initial contact area measurements were discarded to prevent the possibility of error from the slight temperature differences at the interface, with compliance measurements starting at 45 s. Four different temperature gradient samples were monitored for up to 9600 s, and the compliance measured at multiple different temperatures is shown in Fig. 5.

To assemble the master curve, the creep compliance measured at each temperature was shifted with respect to the reference temperature, 22 °C, along the horizontal time axis only. Shift factors, log α_T, were calculated for each shifted data set by matching points of equivalent compliance to determine an average shift factor for the overall data set. We chose this reference temperature in order to compare the shifted data to the previous composition gradient data, which was measured at 22 °C. The compliance master curve using time-temperature superposition is shown in Fig. 6. Shift factors calculated for each temperature scan along with estimated WLF shift factors are shown in Fig. 7. The WLF

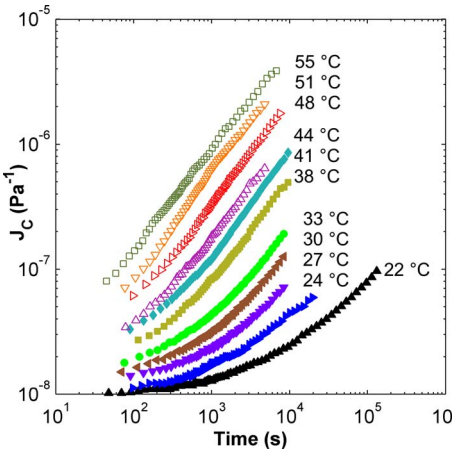

FIG. 5. (Color online) Creep compliance from temperature gradient experiments for 50/50% by mass IBoMA/LMA. The 22 °C temperature experiment measured for 68 h as compared to 2.6 h for the temperature gradient experiments, measured at ten temperatures: 24, 27, 30, 33, 38, 41, 44, 48, 51, and 55 °C.

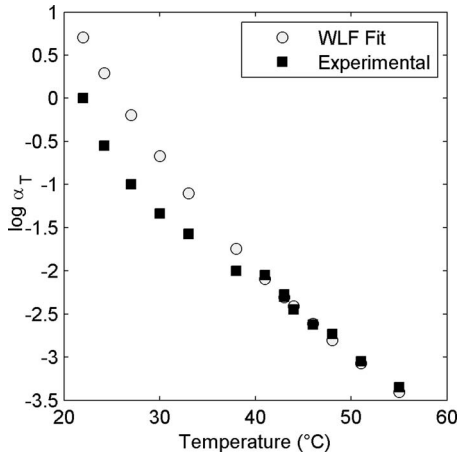

FIG. 7. Shift factors, log α_T, for 50/50% by mass IBoMA/LMA, with WLF predicted shift factors using 22 °C as the reference temperature. WLF predictions are shown for each temperature, fitted only with the shift factors above 40 °C with WLF constants of C_1=9.0 and C_2=73 K.

equation for predicting shift factors is calculated by

$$\log \alpha_T = \frac{-C_1(T-T_R)}{C_2+(T-T_R)}, \tag{3}$$

where T_R is the reference temperature, and C_1 and C_2 are fitted constants for each polymer system. WLF theory is applicable in the temperature range above the glass transition temperature of the polymer, so only shift factors above the glass transition temperature were used to fit the WLF constants. Since the WLF equation is based on a constant free volume change with respect to temperature, the glass transition temperature shift causes prediction errors in WLF shift factors at temperatures below the glass transition temperature. The glass transition temperature, T_G, of 37 °C was obtained using differential scanning calorimetry for this photopolymer composition.

There are multiple advantages to using temperature gradients as compared to a serial experiment version, since this technique requires no further equilibration steps other than forming the initial temperature gradient. With multiple simultaneous measurements, compliance measurements at each temperature allowed for error checking and consistency between shifted data sets. The collapsed master curve is statistically equivalent to the creep compliance measured in the prior step gradient experiment, with the master curve measuring more orders of magnitude while requiring a quarter of the time to perform. The experimental temperature range crossed through the glass transition temperature, causing the experimentally determined shift factors at or below the T_G of the polymer to deviate from the shift factors extrapolated from the WLF fit. In most polymer systems, the WLF equation is applicable when the experimental temperature is above the glass transition temperature, with predictions overestimating the shift factor at temperature lower than the glass transition temperature. The number of temperature scans shown here were significantly higher than a standard time-temperature superposition experiment. Furthermore, the high degree of overlap between measurements offered more potential values for shift factor calculations and further enhanced the accuracy of the shifted data from this technique. This sphere array can be expanded to include more measurements in either direction, either by changing polymer composition as shown in the composition gradient experiments or additional temperature measurements. A single temperature gradient experiment measuring four different temperatures with three repeats each could replicate the master curve assembled in Fig. 6, taking a total of 3.5 h to complete.

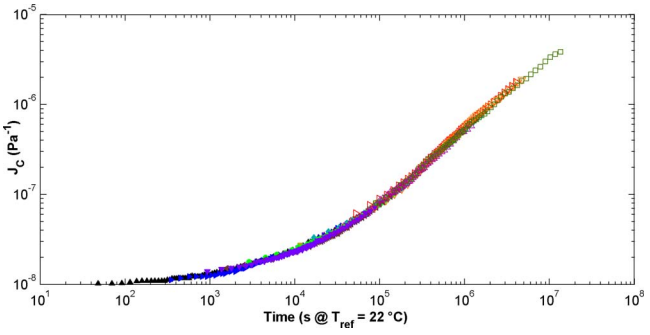

FIG. 6. (Color online) Creep compliance master curve for 50/50% by mass IBoMA/LMA using time-temperature superposition. Shift factors are given in Fig. 7, with all curves shifted to a time corresponding to a reference temperature of 22 °C.

Through the use of simple contact geometry and independent probes, a high-throughput methodology for determining the viscoelastic properties of polymers has been developed using surface indentation. Our measurements show agreement with well-established, viscoelastic measurement techniques and retain a high degree of accuracy by measuring contact area instead of penetration depth. Moreover, our technique provides higher accuracy since repeat measurements can be made within the same experimental scan. To demonstrate markedly different creep compliances within the same sample, compositional step gradient samples with changes in polymer composition were produced, which showed trends in creep compliance consistent with expected theory. In addition, time-temperature superposition was demonstrated, generating shift factors and a master curve for a

polymer system by leveraging a temperature gradient to obtain repeated measurements for multiple temperatures within a single experiment. With independent sample conditions for each indenting sphere, viscoelastic properties with varying conditions were investigated within the same experiment.

ACKNOWLEDGMENTS

P.M.J. gratefully acknowledges support from the National Research Council Postdoctoral Research Associate program.

[1] C. A. Angell, K. L. Ngai, G. B. McKenna, P. F. McMillan, and S. W. Martin, J. Appl. Phys. **88**, 3113 (2000).
[2] P. A. O'Connell and G. B. McKenna, Science **307**, 1760 (2005).
[3] D. C. Lin and F. Horkay, Soft Matter **4**, 669 (2008).
[4] C. C. White, M. R. Vanlandingham, P. L. Drzal, N. K. Chang, and S. H. Chang, J. Polym. Sci., Part B: Polym. Phys. **43**, 1812 (2005).
[5] M. R. VanLandingham, N. K. Chang, P. L. Drzal, C. C. White, and S. H. Chang, J. Polym. Sci., Part B: Polym. Phys. **43**, 1794 (2005).
[6] C. A. Tweedie and K. J. Van Vliet, J. Mater. Res. **21**, 1576 (2006).
[7] G. A. Bell, D. M. Bielinski, and B. D. Beake, J. Appl. Polym. Sci. **107**, 577 (2008).
[8] M. L. Williams, J. Phys. Chem. **59**, 95 (1955).
[9] S. S. Es-Haghi, A. A. Yousefi, and A. Oromiehie, J. Polym. Sci., Part B: Polym. Phys. **45**, 2860 (2007).
[10] J. L. Yang, Z. Zhang, A. K. Schlarb, and K. Friedrich, Polymer **47**, 6745 (2006).
[11] K. L. Ngai and D. J. Plazek, Macromolecules **23**, 4282 (1990).
[12] M. Ganß, B. K. Satapathy, M. Thunga, R. Weidisch, P. Potschke, and A. Janke, Macromol. Rapid Commun. **28**, 1624 (2007).
[13] C. J. Perez, V. A. Alvarez, and A. Vazquez, Mater. Sci. Eng., A **480**, 259 (2008).
[14] J. D. Ferry, *Viscoelastic Properties of Polymers* (Wiley, New York, 1980).
[15] P. A. O'Connell and G. B. McKenna, Polym. Eng. Sci. **37**, 1485 (1997).
[16] R. Jayachandran, M. C. Boyce, and A. S. Argon, J. Adhes. Sci. Technol. **7**, 813 (1993).
[17] E. H. Lee and J. R. M. Radok, J. Appl. Mech. **27**, 438 (1960).
[18] J. Illingworth and J. Kittler, Comput. Vis. Graph. Image Process. **44**, 87 (1988).
[19] D. H. Ballard, Pattern Recogn. **13**, 111 (1981).
[20] J. Canny, IEEE Trans. Pattern Anal. Mach. Intell. **8**, 679 (1986).
[21] V. Rek, T. H. Grguric, and Z. Jelcic, Macromol. Symp. **202**, 127 (2003).
[22] J. C. Meredith, A. Karim, and E. J. Amis, Macromolecules **33**, 5760 (2000).